Journal of Physics and Chemistry of Solids 69 (2008) 2674–2680

Contents lists available at ScienceDirect

Journal of Physics and Chemistry of Solids

journal homepage: www.elsevier.com/locate/jpcs

$BaMoO_4$ powders processed in domestic microwave-hydrothermal: Synthesis, characterization and photoluminescence at room temperature

L.S. Cavalcante [a,*], J.C. Sczancoski [a], R.L. Tranquilin [a], M.R. Joya [a], P.S. Pizani [a], J.A. Varela [b], E. Longo [b]

[a] LIEC-UFSCar, Departamento de Química e Física, P.O. Box 676, 13565-905 São Carlos, SP, Brazil
[b] LIEC-UNESP, Instituto de de Química, P.O. Box 355, 14801-907 Araraquara, SP, Brazil

ARTICLE INFO

Article history:
Received 19 December 2007
Received in revised form
17 May 2008
Accepted 17 June 2008

Keywords:
A. Optical materials
B. Chemical synthesis
C. Electron microscopy
D. Luminescence
D. Optical properties

ABSTRACT

In this paper, $BaMoO_4$ powders were prepared by the coprecipitation method and processed in a domestic microwave-hydrothermal. The obtained powders were characterized by X-ray diffraction (XRD), Fourier transform Raman (FT-Raman) spectroscopy, ultraviolet–visible (UV–vis) absorption spectroscopy and photoluminescence (PL) measurements. The morphology of these powders were investigated by scanning electron microscopy (SEM). SEM micrographs showed that the $BaMoO_4$ powders present a polydisperse particle size distribution. XRD and FT-Raman analyses revealed that the $BaMoO_4$ powders are free of secondary phases and crystallize in a tetragonal structure. UV–vis was employed to determine the optical band gap of this material. PL measurements at room temperature exhibited a maximum emission around 542 nm (green emission) when excited with 488 nm wavelength. This PL behavior was attributed to the existence of intrinsic distortions into the $[MoO_4]$ tetrahedron groups in the lattice.

1. Introduction

Barium molybdate, $BaMoO_4$, presents at room temperature a scheelite-type tetragonal structure with general formula $[AXO_4]$, where A = Ca, Sr, Ba and X = Mo [1,2]. This compound has been prepared by the conventional solid-state reaction between $BaCO_3$ and MoO_3 at high temperatures ($\gg 1200\,^{\circ}C$) [3]. $BaMoO_4$ obtained for this method presents several problems, such as: inhomogeneity, contamination by impurities and nonuniform particle size distribution [4]. Other methods also have been employed to prepare the $BaMoO_4$, including as flux crystallization [5], Czochralski technique [6] and spontaneous crystallization (SC) [7]. However, the main drawback of these techniques is the high processing temperature. To minimize these problems, wet chemical methods have been utilized, including polymerized complex [8], citrate complex method [9] and electrochemical method [10]. In addition, hydrothermal processing is considered an efficient and versatile method for the formation of several nanostructured materials with different morphologies and sizes. Recently, methods as solvothermal [11] and conventional hydrothermal (CHT) [12] have been used to process $BaMoO_4$ at temperatures in the range from 100 to 200 °C for times from 12 to 24 h. The microwave radiation has been employed in the citrate complex and solvothermal methods to accelerate the reaction process in the formation of molybdates with scheelite-type structure [13,14]. In the case of microwave-hydrothermal processing, the high frequency electromagnetic radiation interacts with the permanent dipole of the liquid (H_2O), which initiates a rapid heating from the resultant molecular rotation. Likewise, permanent or induced dipoles in the dispersed phase cause rapid heating of the particles. These result in a reaction temperature in excess of the surrounding liquid-localized superheating [15]. Thus, microwave radiation is able to promote the formation of materials with short processing time and reduced electric energy cost [16].

The literature has reported the formation of several amorphous compounds based on different metal oxianions with intense photoluminescence (PL) at room temperature [17–19]. In particular, an important material with scheelite-type structure is the $BaMoO_4$, which presents a high technological potential due to their blue photoluminescence (PL) property [20]. Recently, Marques et al. [8,21] reported the PL properties of amorphous $BaMoO_4$ in thin film and powders. PL properties were also verified in well-crystallized $BaMoO_4$ films [22].

Therefore, in this paper, we report on the preparation of $BaMoO_4$ powders by the coprecipitation method and processed in a domestic microwave-hydrothermal (DMW-HT) at 140 °C for 1 h. These powders were structurally characterized by X-ray diffraction (XRD) and Fourier transform Raman (FT-Raman) spectroscopy. The morphology was investigated by scanning electronic microscopy (SEM). The optical properties were analyzed by

* Corresponding author. Tel.: +55 16 3361 5215, Mob.: +55 16 9176 4943; fax: +55 16 3351 8214.
E-mail address: laeciosc@bol.com.br (L.S. Cavalcante).

0022-3697/$ - see front matter © 2008 Elsevier Ltd. All rights reserved.
doi:10.1016/j.jpcs.2008.06.107

ultraviolet–visible (UV–vis) absorption spectroscopy and photoluminescence (PL) measurements at room temperature.

2. Experimental details

2.1. Synthesis and processing of $BaMoO_4$ powders

$BaMoO_4$ powders were synthesized by the coprecipitation method [23] and processed in a DMW-HT at 140 °C for 1 h in the presence of polyethylene glycol (PEG). A typical experimental procedure to obtain $BaMoO_4$ powders is illustrated in Fig. 1.

About 5×10^{-3} mol of molybdic acid [H_2MoO_4] (85% purity, Synth), 5×10^{-3} mol of barium nitrate [$Ba(NO_3)_2$] (99.5% purity, Sigma-Aldrich), NH_4OH (30% in NH_3, Synth) and 0.1 g of PEG (*Mw* 200) (99.9% purity, Sigma-Aldrich) were used as raw materials. The solubilization of tungstic acid and barium salt in water can be observed in Fig. 1. The insert shows the precipitation reaction between H_2MoO_4 and $Ba(NO_3)_2$ for the formation of the first particles of $BaMoO_4$. This solution containing H_2MoO_4 and $Ba(NO_3)_2$ was stirred for 1 h. This procedure was employed to accelerate the coprecipitation rate of $BaMoO_4$. Then, the following, 5 mL of NH_4OH was added in this solution to intensify the hydrolysis rate between the metal acid and the salt in water. In this case, the Ba^{2+} cations are accept species of electron pairs (Lewis acid) while MoO_4^{2-} are donor species of electron pairs (Lewis base). The reactions between these two species $Ba^{2+} \leftarrow: MO_4^{2-}$ form a covalent bond. The covalent bond occurs due to the Lewis acid to occupy the lowest molecular orbital (LUMO), which interacts with the highest molecular orbital (HOMO) of the Lewis base. Afterwards 0.1 g of PEG was added into this solution to promote a interaction between the small particles. In the sequence, the chemical solution was stirred for 30 min in ultrasound at room temperature was transferred into a Teflon autoclave, which was sealed and placed into a DMW-HT (2.45 GHz, maximum power of 800 W). This system was kept at 140 °C for 1 h, using a heating rate fixed at 25 °C/min. The pressure into the autoclave was stabilized at 3.92 bar. After microwave-hydrothermal processing, the autoclave was cooled to room temperature naturally. The obtained powders were then collected and washed with deionized water several times and then slowly dried at 85 °C for some hours.

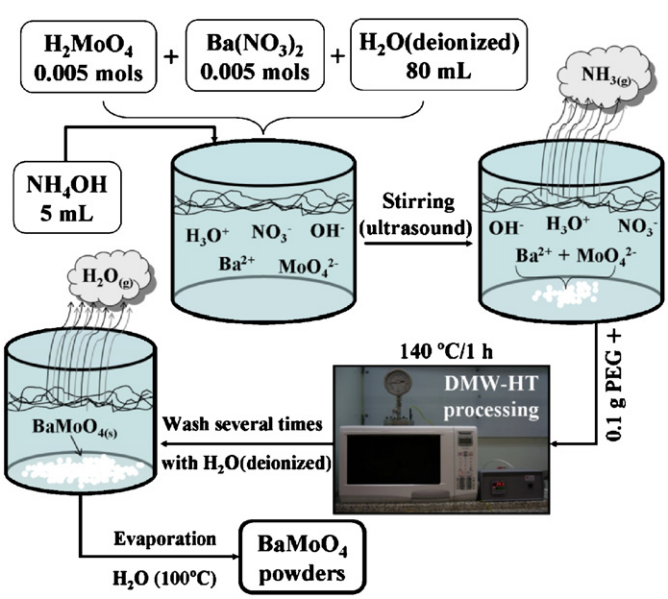

Fig. 1. Flow-chart illustrating the experimental procedure for the formation of $BaMoO_4$ powders.

2.2. Characterizations

$BaMoO_4$ powders were characterized by XRD patterns recorded on a (Rigaku-DMax 2500PC, Japan) with Cu-Kα radiation in the 2θ range from 5° to 75° with 0.02°/min. FT-Raman spectroscopy was performed on Bruker-RFS 100, Germany. The spectra were obtained using a 1064 nm line of an Nd:YAG laser, keeping their maximum output power at 55 mW. The morphology of these powders was observed through an scanning electron microscopy [DSM940A, Carl Zeiss, Germany]. UV–vis spectroscopy was taken using a (Cary 5G equipment, USA). PL spectra were taken with a (U1000 Jobin-Yvon, France) double monochromator coupled to a cooled GaAs photomultiplier with conventional photon counting system. The 488.0 nm excitation wavelength of an argon ion laser was used, keeping their maximum output power at 25 mW. A cylindrical lens was used to prevent overheating of the powders. The slit width used was 100 μm. All measurements were performed at room temperature.

3. Results and discussion

3.1. X-ray diffraction analysis

Fig. 2 shows the XRD patterns of $BaMoO_4$ powders processed in DMW-HT at 140 °C for 1 h.

The presence of diffraction peaks can be used to evaluate the structural order at long-range or periodicity of the material. All diffraction peaks can be indexed to the scheelite-type tetragonal structure with space group $I4_1/a$ [24]. No additional phase peaks were observed. The lattice parameters were calculated using the least square refinement from the UNITCELL-97 program [25]. The obtained lattice parameters were $a = b = 5.5696$ Å and $c = 12.7865$ Å with an unit cell volume of 396.642(8) Å^3. These values are in agreement with those reported in the literature and with the respective JCPDS (Joint Committee on Powder Diffraction Standards) card No. 29-0193 [26].

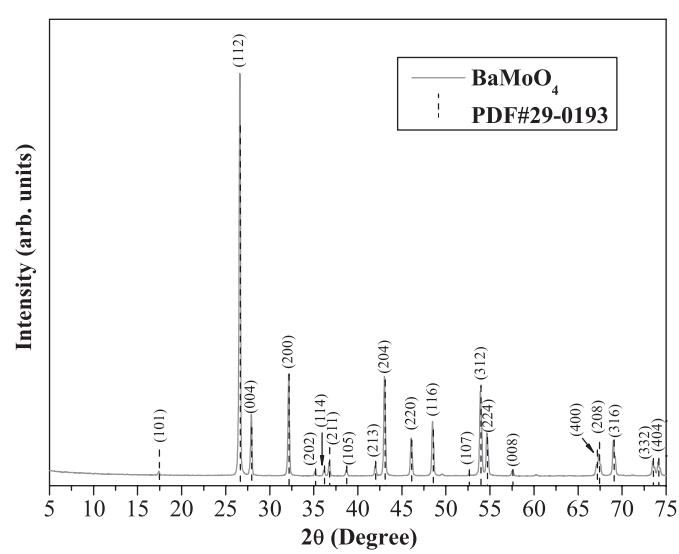

Fig. 2. XRD patterns of $BaMoO_4$ powders processed in a domestic microwave-hydrothermal at 140 °C for 1 h. The vertical dashed lines indicate the position and relative intensity of the respective JCPDS card no. 29-0193.

Table 1
Comparative results between the lattice parameters of $BaMoO_4$ obtained in this work with those reported in the literature by different methods

T (°C)	Time (h)	Average lattice $a = b$ (Å)	Parameter c (Å)	Method	Reference
1200	40	5.62	12.82	Czochralski	[6]
950	72	–	–	SC	[7]
700	2	5.579(1)	12.811(4)	CPM	[8]
1150	12	5.5479(9)	12.743(2)	Precipitation/calcination	[31]
550	12	–	–	Molten flux reaction	[37]
140	1	5.569(6)	12.786(5)	DMW-HT	[This work]

T, temperature; CPM, complex polymerization method; SC, spontaneous crystallization and DMW-HT, domestic microwave-hydrothermal.

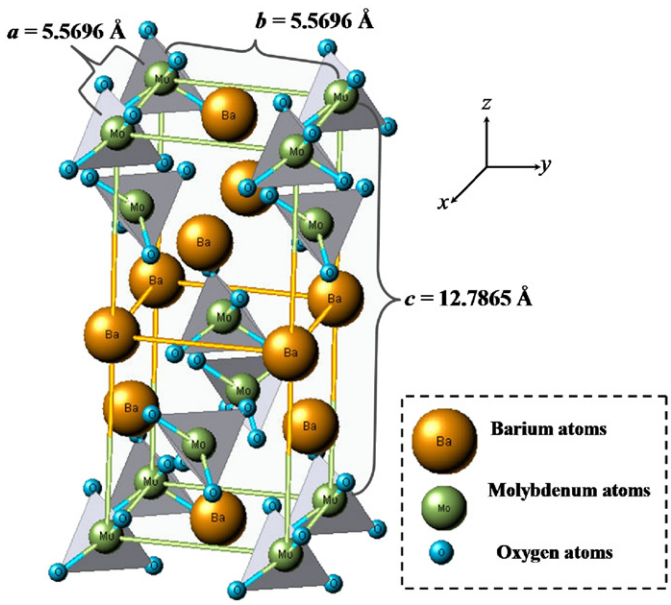

Fig. 3. $1 \times 1 \times 1$ unit cell of $BaMoO_4$ tetragonal structure.

Table 1 shows a comparative between the lattice parameters values of $BaMoO_4$ obtained in this work with other methods reported in the literature.

As can be seen in Table 1, the preparation of $BaMoO_4$ powders in a DMW-HT system leads to a reduction of temperature and processing time. Compared with the usual methods, the microwave processing is able to promote the formation of materials with small particle sizes, narrow particle size distribution and high purity. Jansen et al. [27] reported that these advantages could be attributed to the fast homogeneous nucleation and easy dissolution of the particles in the sol–gel system.

3.2. Unit cell representation for $BaMoO_4$

Fig. 3 illustrates the schematic representation of $BaMoO_4$ tetragonal unit cell with $I4_1/a$ space group. The Java Structure Viewer Program (Version 1.08lite for Windows) [28] was used for modeling this unit cell.

For construction of $1 \times 1 \times 1$ unit cell of $BaMoO_4$ as showed in Fig. 3, we employed the structural parameters and atomic coordinates listed in Table 2 [29,30]. Nassif et al. [31] showed that Ba^{2+} cations are coordinated to the eight oxygen atoms, forming a scalenohedra configuration. The oxygen coordination polyhedra of Mo^{6+} cations are slightly distorted tetrahedral, presenting the angles between oxygen of 108.3° and 111.83°. For visual effect, our unit cell shows only the coordination between Mo–O atoms.

Table 2
Atomic coordinates used to model the $BaMoO_4$ unit cell

Atom	Site	x	y	z
Molybdenum	4a	0	0	0
Barium	4b	0	0	0.5
Oxygen	16f	0.76731	0.14013	0.08188

$a = b = 5.5696$ Å and $c = 12.7865$ Å.

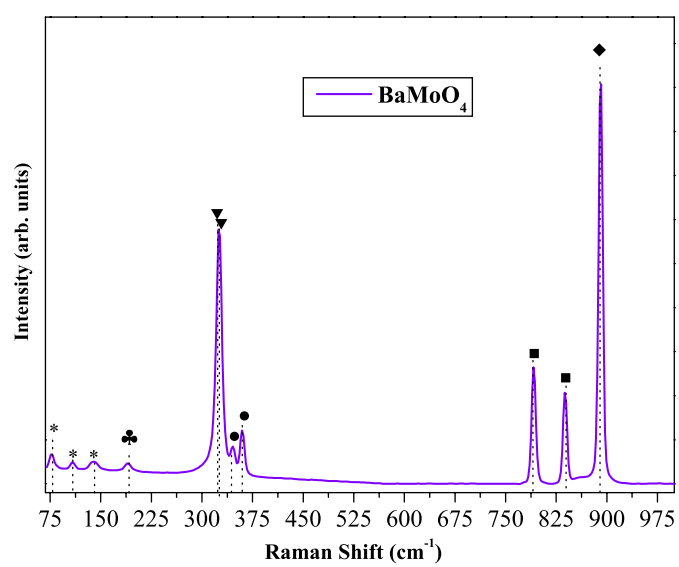

Fig. 4. Raman spectrum of $BaMoO_4$ powders processed in a domestic microwave-hydrothermal at 140 °C for 1 h.

3.3. FT-Raman spectroscopy analysis

Fig. 4 shows the Raman spectrum in the range from 68 cm^{-1} to 1000 cm^{-1} for the $BaMoO_4$ powders processed in a DMW-HT at 140 °C for 1 h.

$BaMoO_4$ presents a tetragonal structure with symmetry C_{4h}^6 at room temperature. According to group theory calculation, the $BaMoO_4$ presents 26 different vibrations as described by the following equation:

$$\Gamma = 3A_g + 5A_u + 5B_g + 3B_u + 5E_g + 5E_u, \quad (1)$$

where all the even vibrations (A_g, B_g and E_g) are Raman-active modes, while the odd modes ($4A_u$ and $4E_u$) can be only verified in the infrared spectra. The three B_u vibrations are silent modes. Eq. (1) also includes one A_u and one E_u acoustic vibrations [6]. According to Porto and Scott [32] the molybdates are classified into two groups, the external and internal modes. The first is

Table 3
Comparative results between the Raman-active modes of $BaMoO_4$ obtained in this work with those reported in the literature by different methods

M	T (°C)	t h	B_g *	E_g *	B_g *	E_g ♣	A_g ▼	B_g ▼	B_g •	E_g •	E_g ■	B_g ■	A_g ◆	Ref.
DMW-HT	140	1	78	109	140	190	325	327	346	340	791	838	892	[This work]
CZ	1200	40	76	110	137	188	234	324	345	358	791	837	892	[6]
CPM	700	2	78	107	141	190	325	326	346	359	791	838	891	[8]
MWS	165	$\frac{1}{3}$	–	–	–	184	–	325	–	362	780	829	871	[14]

M, method; T, temperature; t, time; assignments modes: ∗, v_{ext}-external modes MoO_4^{2-} and Ba^{2+} motions; ♣, $v_{f.r}(F_1)$ free rotation; ▼, $v_2(E)$; •, v_4 (F_2); ■, $v_3(F_2)$; ◆, $v_1(A_1)$; methods of preparation: DMW-HT, domestic microwave-hydrothermal; CPM, complex polymerization method; CZ, Czocharalski method and MWS, microwave-solvothermal process and Ref., references.

called lattice phonon, which corresponds to the motion of Ba^{2+} cations and the rigid molecular units. The second belong to the vibration inside $[MoO_4]^{2-}$ molecular units with the center mass stationary. In free space, $[MoO_4]^{2-}$ tetrahedrons present a cubic point symmetry T_d [6]. Their vibrations are composed by four internal modes ($v_1(A_1)$, $v_2(E_1)$, $v_3(F_2)$ and $v_4(F_2)$), one free rotation mode and one translation mode (F_2) [6].

Table 3 shows a comparative between the Raman modes of $BaMoO_4$ obtained in this work with those reported in the literature by different methods.

In Table 3, it was verified that all Raman-active modes are characteristic of $BaMoO_4$ phase in agreement with the reported in the literature [6,8]. Therefore, these results confirm the tetragonal structure for the $BaMoO_4$ powders. The small variations can be associated with the preparation method, average crystal size and structural order degree. The presence of Raman-active modes can be used to evaluate the structural order at short-range of the materials. Thongtem et al. [14] observed the presence of only six Raman-active modes for the $BaMoO_4$ formed through cyclic microwave radiation. Thus, our results show the presence of Raman-active modes indicated that the $BaMoO_4$ powders are completely ordered at short-range. Possibly, these differences are caused by the preparation method, geometry and/or particle size.

3.4. Scanning electron microscope analysis

$BaMoO_4$ powders with octahedral morphology was observed through the scanning electron microscope (SEM), as shown in Fig. 5.

Fig. 5(a) shows the SEM micrographs of the $BaMoO_4$ powders. The micrographs revealed the presence of $BaMoO_4$ powders with agglomerate nature and with different particle size distribution. A projection set of $BaMoO_4$ powders is indicated by the dotted white circle (see Fig. 5(b)). Therefore, obtained micrographs show that the microwave irradiation contribute significantly for the formation of $BaMoO_4$ powders with short processing time. The PEG promoted a increase in the aggregation process of small particles or nucleation seeds on the surface through the lateral interaction of hydrogen bonding of water with the OH groups of this polymer. In Fig. 5(c) the dotted white circles show four different regions of $BaMoO_4$ powders. As can be seen in this figure, initially several small particles or seeds act as small nucleation centers during the DMW-HT processing (see Fig. 5(d)). Fig. 5(e) shows the polydisperse particle size distribution of $BaMoO_4$ powders processed in a DMW-HT system. The coalescence process is indicated by dotted white ellipses. A possible growth mechanism occurs through the coalescence process between small and large particles during the DMW-HT processing (arrows in Fig. 5(f)). Our proposed mechanism for the formation of particles with octahedron-like morphology is in agreement with those reported in the literature [33–35].

The average particle size distribution were obtained through the SEM micrographs by the counting of approximately 102 particles, as illustrated in Fig. 6.

The average particle size of $BaMoO_4$ powders in the range from 0.7 μm to 3.1 μm present as tendency a regular lognormal distribution. The higher frequency (%) of particles was approximately 1.3 μm. This distribution is asymmetrical on the logarithmic scale of average particle size. This system presents the microcrystallites with an octahedron-like morphology and polydisperse particle size distribution.

3.5. UV– vis absorption spectroscopy analysis

Fig. 7 shows a typical UV–vis spectrum of $BaMoO_4$ powders processed in a DMW-HT at 140 °C for 1 h. The obtained optical band gap value is shown in Fig. 7 and listed in Table 4.

The optical band gap (E_g) was estimated by the method proposed by Wood and Tauc [36]. According to these authors, the optical band gap energy is associated with absorbance and photon energy by the following equation:

$$h\nu\alpha \propto (h\nu - E_g^{opt})^{1/2}, \quad (2)$$

where α is the absorbance, h is the Planck constant, ν is the frequency, and E_g^{opt} is the optical band gap.

In this case, E_g value was determinate extrapolating the linear portion of the curve or tail. The combination between the optical band gap and PL measurements allows to correlated that electronic transitions in the materials. UV–vis measurements revealed a typical value of 4.10 eV for the $BaMoO_4$ powders. This observed behavior can be associated with the energy difference between the valence band and conduction band for this material. The obtained result was similar to that reported by Afanasiev [37] and Eng et al. [38]. The fast processing in microwave-hydrothermal can lead to the formation of possible defects in $BaMoO_4$ lattice, thus promoting the appearance of intermediate electronic levels in the band gap. Table 4 shows a comparative between E_g values of $BaMoO_4$ obtained in this work with those reported in the literature by different methods.

The differences verified in the optical band gap values can be related with the different preparation methods, shape, average crystal size and structural order–disorder degree in the lattice. As can be seen in Table 4, the E_g value is slightly lower than obtained by Marques et al. for $BaMoO_4$ thin films [21]. According to Eng et al. [38] the E_g values in material is dependent upon the electronegativity of the transition metal ion, connectivity of the polyhedra and deviations in the O–Mo–O bonds.

3.6. PL analysis

Fig. 8 shows the PL spectrum of $BaMoO_4$ powders processed in a DMW-HT at 140 °C for 1 h. The maximum (PL) emission was observed at around 542 nm (green emission).

PL measurements were realized at room temperature because this optical property behavior can be influenced by the temperature. Moreover, PL measurements at different

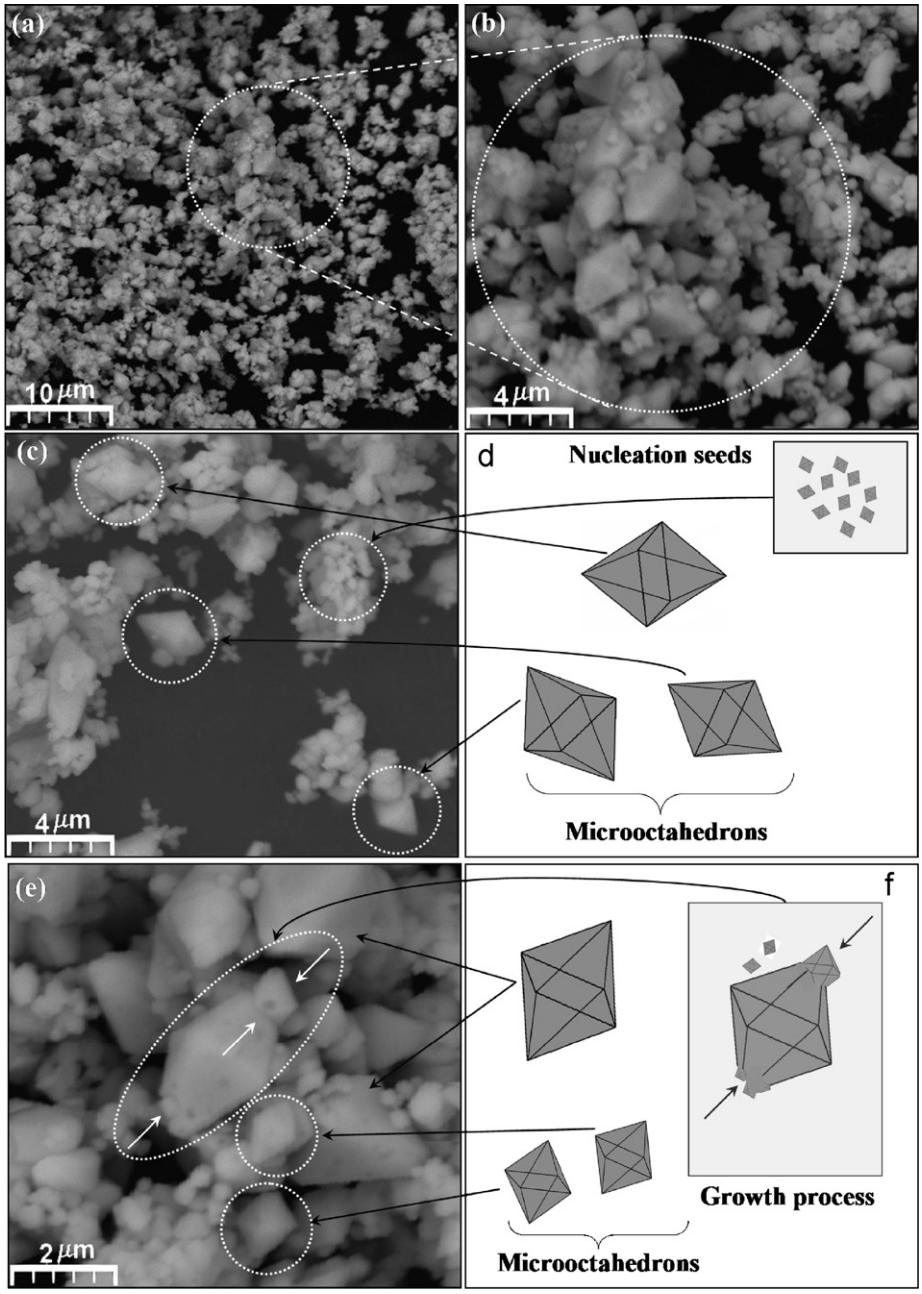

Fig. 5. SEM micrographs: (a) $BaMoO_4$ powders processed in DMW-HT at 140 °C for 1 h, (b) selected region of an agglomerated of $BaMoO_4$ powders, (c) polydisperse particle size distribution, (d) nucleation process by small seeds, (e) coalescence process and (f) possible growth mechanism of $BaMoO_4$ powders in a domenstic microwave-hydrothermal.

temperatures generally require expensive and sophisticated equipments. Also, it is technologically more interesting the materials with PL emissions at room temperature for the development of electrooptic devices, including DVD player lasers, cell phone displays, photocopying lamps and so on. The literature has reported explanations on PL emissions of molybdates. Lan and Blasse [39] prepared $BaMoO_4$ using $Ba(NO_3)_2$ and Na_2MoO_4 solutions. These authors observed that $BaMoO_4$ exhibit a weak green emission (around 530 nm) at −268.8 °C. This green emission was also verified by Spassky et al. [7], with the maximum emission around 520 nm at −263 °C. Both authors attributed the green luminescence of $BaMoO_4$ with the intrinsic MoO_4^{2-} group. Ryu et al. [9] reported the great dependence of the PL properties on the morphology and crystallinity of the $BaMoO_4$ powders. Recently, Campos et al. [17] observed and reported the green PL emission in calcium molybdate and attributed this behavior to the intrinsic distortions into the $[MoO_4]$ tetrahedron groups. In other work, Wu et al. [20] investigated the blue PL emission at room temperature of $BaMoO_4$ microcrystals and show that slightly distorted tetrahedral symmetry leads to an structured absorption band for the $A_1 \rightarrow T_{1(2)}$ transition. Marques et al. [40] attributed the green PL emission to structural disorder in the MoO_4 cluster for the $BaMoO_4$ powders obtained by the complex polymerization method. Liu et al. [41] attributed to the charge-transfer transitions within the $[MoO_4]^{2-}$ complex to mainly factor to green PL emission in barium molybdate. We believe that the green PL emission at room temperature in barium molybdate is linked a several factors, such as: distortions on the $[MoO_4]$ tetrahedron groups caused by the different angles between O–Mo–O (108.3° and 111.8°), particle sizes, crystallinity degree, morphology and

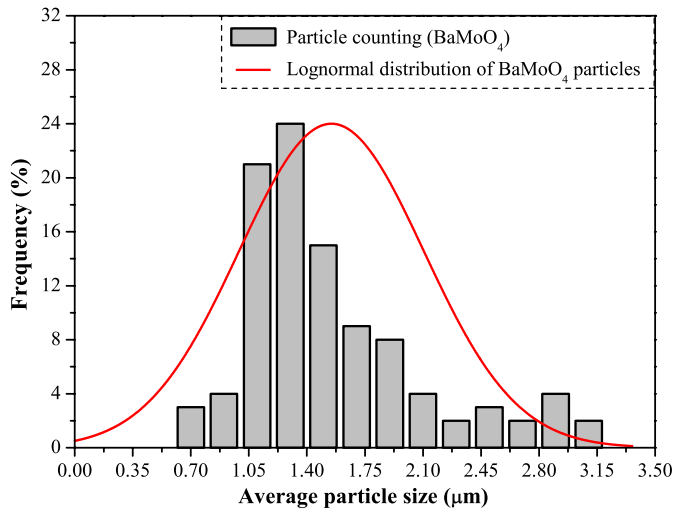

Fig. 6. Average particle size distribution of $BaMoO_4$ powders processed in a domestic microwave-hydrothermal at 140 °C for 1 h.

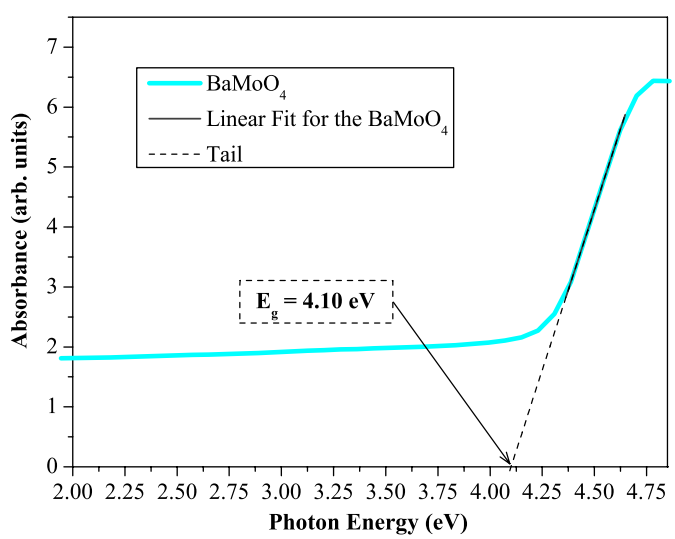

Fig. 7. UV–vis absorbance spectra for the $BaMoO_4$ powders processed in a domestic microwave-hydrothermal at 140 °C for 1 h.

Table 4
Comparative results between the optical band gap energy of $BaMoO_4$ obtained in this work with those reported in the literature by different methods

Temperature (°C)	140	600	200	200	550	1300
Time (h)	1	2	4	16	12	12
Optical gap (eV)	4.10	4.88	4.73	4.82	4.30	4.00
Reference	This work	[21]	[21]	[21]	[37]	[38]

surface defects. In this case, these factors promote the formation of visible light emission centers responsible by the PL property of this material.

4. Conclusions

In summary, $BaMoO_4$ powders were obtained by the coprecipitation and processed at 140 °C for 1 h in a domestic microwave-hydrothermal system. XRD patterns and FT-Raman revealed that the $BaMoO_4$ powders present a scheelite-type tetragonal structure without the presence of secondary phases. UV–vis absorption

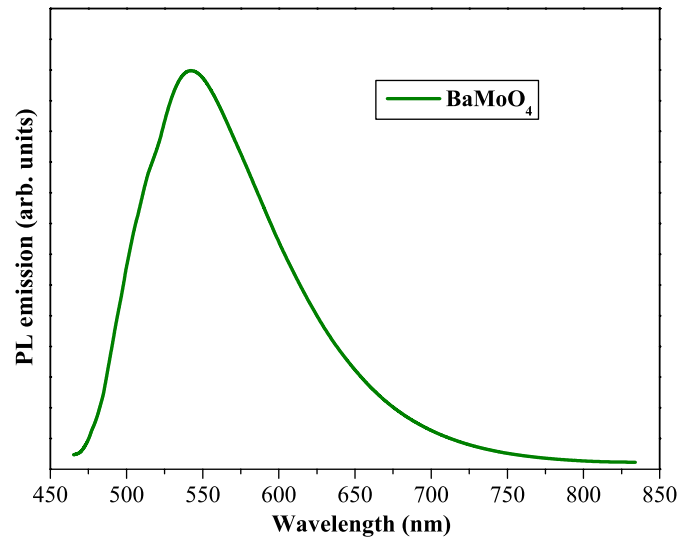

Fig. 8. PL spectrum at room temperature of $BaMoO_4$ powders processed in a domestic microwave-hydrothermal at 140 °C for 1 h excited with the 488 nm line of an argon ion laser.

spectroscopy revealed a characteristic optical band gap of 4.10 eV. SEM micrographs showed that the $BaMoO_4$ powders present a polydisperse particle size distribution. These micrographs also showed that the coalescence mechanism is responsible by the growth process of $BaMoO_4$ with octahedron-like morphology. Intense PL emission at room temperature was attributed to the distortions on the $[MoO_4]$ tetrahedron groups, particle sizes, crystallinity degree, morphology and surface defects.

Acknowledgments

The authors thank the financial support of the Brazilian research financing institutions: CAPES, FAPESP, CNPq and also Prof. Dr. Dawy Keyson-UFPB and Dr. Diogo P. Volanti by adaptation of the hydrothermal reactor in the domestic microwave.

References

[1] V. Thangadurai, C. Knittlmayer, W. Weppner, Mater. Sci. Eng. B 106 (2004) 228.
[2] J.-W. Yoon, J.H. Ryu, Mater. Sci. Eng. B 127 (2006) 154.
[3] C. Pupp, R. Yamdagni, R.F. Porter, J. Inorg. Nucl. Chem. 31 (1969) 2021.
[4] L.A. Al-Hajji, M.A. Hasan, M.I. Zaki, J. Mater. Res. 18 (2003) 2339.
[5] S.K. Arora, G.S.T. Rao, J. Cryst. Growth 53 (1981) 627.
[6] T.T. Basiev, A.A. Sobol, Y.U.K. Voronko, P.G. Zverev, Opt. Mater. 15 (2000) 205.
[7] D.A. Spassky, S.N. Ivanov, V.N. Kolobanov, V.V. Mikhailin, V.N. Zemskov, B.I. Zadneprovski, L.I. Potkin, Radiat. Meas. 38 (2004) 607.
[8] A.P.A. Marques, D.M.A. de Melo, C.A. Paskocimas, P.S. Pizani, M.R. Joya, E.R. Leite, E. Longo, J. Solid State Chem. 179 (2006) 671.
[9] J.H. Ryu, J.-W. Yoon, C.J. Lim, K.B. Shim, Mater. Res. Bull. 40 (2005) 1468.
[10] J. Bi, D.Q. Xiao, D.J. Gao, P. Yu, G.L. Yu, W. Zhang, J.G. Zhu, Crys. Res. Technol. 38 (2003) 935.
[11] C. Zhang, E. Shen, E. Wang, Z. Kang, L. Gao, C. Hu, L. Xu, Mater. Chem. Phys. 96 (2006) 240.
[12] M. Yoshimura, J. Mater. Sci. 41 (2006) 1299.
[13] J.H. Ryu, J.-W. Yoon, K.B. Shim, J. Alloys Compd. 413 (2006) 144.
[14] T. Thongtem, A. Phuruangrat, S. Thongtem, Mater. Lett. 62 (2008) 454.
[15] G.J. Wilson, A.S. Matijasevich, D.R.G. Mitchell, J.C. Schulz, G.D. Will, Langmuir 22 (2006) 2016.
[16] D. Keyson, D.P. Volanti, L.S. Cavalcante, A.Z. Simões, I.A. Souza, J.S. Vasconcelos, J.A. Varela, E. Longo, J. Mater. Process. Technol. 189 (2007) 316.
[17] A.B. Campos, A.Z. Simões, E. Longo, J.A. Varela, V.M. Longo, A.T. de Figueiredo, F.S. De Vicente, A.C. Hernandes, Appl. Phys. Lett. 91 (2007) 051923.
[18] M. Anicete-Santos, F.C. Picon, M.T. Escote, E.R. Leite, P.S. Pizani, J.A. Varela, E. Longo, Appl. Phys. Lett. 88 (2006) 211913.
[19] R.C. Lima, M. Anicete-Santos, E. Orhan, M.A.M.A. Maurera, A.G. Souza, P.S. Pizani, E.R. Leite, J.A. Varela, E. Longo, J. Lumin. 126 (2007) 741.
[20] X. Wu, J. Du, H. Li, M. Zhang, B. Xi, H. Fan, Y. Zhu, Y. Qian, J. Solid State Chem. 180 (2007) 3288.

[21] A.P.A. Marques, D.M.A. de Melo, E. Longo, C.A. Paskocimas, P.S. Pizani, E.R. Leite, J. Solid State Chem. 178 (2005) 2346.
[22] C. Cui, J. Bi, F. Shi, X. Lai, D. Gao, Mater. Lett. 61 (2007) 4525.
[23] M.J. Godinho, R.F. Gonçalves, L.P.S. Santos, J.A. Varela, E. Longo, E.R. Leite, Mater. Lett. 61 (2007) 1904.
[24] J.C. Sczancoski, L.S. Cavalcante, M.R. Joya, J.A. Varela, P.S. Pizani, E. Longo, Chem. Eng. J. 140 (2008) 632.
[25] T.J.B. Holland, S.A.T. Redfern, Miner. Mag. 61 (1997) 65.
[26] ⟨www.icdd.com/profile/overview.htm⟩.
[27] C. Jansen, A. Arafat, A.K. Barakat, H. Van Bekkum, in: M.L. Occelli, H. Robson (Eds.), Synthesis of Microporous Materials, vol. 1, Van Nostrand Reinhold, New York, 1992, p. 507.
[28] ⟨http://www.jcrystal.com/steffenweber/JAVA/JSV/jsv.html⟩.
[29] J. Leciejewicz, Z. Kristallogr. 121 (1965) 158.
[30] S. Takai, S. Touda, K. Oikawa, K. Mori, S. Torii, S. Torii, T. Kamiyama, T. Esaka, Solid State Ion. 148 (2007) 123.
[31] V. Nassif, R.E. Carbonio, J. Solid State Chem. 146 (1999) 266.
[32] S.P.S. Porto, J.F. Scott, Phys. Rev. 157 (1967) 716.
[33] E.-K. Ryu, Y.-D. Huh, Bull. Korean Chem. Soc. 29 (2008) 503.
[34] Q. Gong, X. Qian, H. Cao, W. Du, X. Ma, M. Mo, J. Phys. Chem. B 110 (2006) 19295.
[35] X. Zhao, T.L.Y. Cheung, Y. Xi, K.C. Chung, D.H.L. Ng, J. Yu, J. Mater. Sci. 42 (2007) 6716.
[36] D.L. Wood, J. Tauc, Phys. Rev. 5 (1972) 3144.
[37] P. Afanasiev, Mater. Lett. 61 (2007) 4622.
[38] H.W. Eng, P.W. Barnes, B.M. Auer, P.M. Woodward, J. Solid State Chem. 175 (2003) 94.
[39] R.U.E. 't Lan, G. Blasse, J. Phys. Chem. 71 (1979) 3549.
[40] A.P.A. Marques, F.C. Picon, D.M.A. Melo, P.S. Pizani, E.R. Leite, J.A. Varela, E. Longo, J. Fluoresc. 18 (2008) 51.
[41] J. Liu, X. Huang, Y. Li, Z. Li, J. Mater. Chem. 17 (2007) 2754.